


Doppler-free two-photon cavity ring-down spectroscopy of a nitrous oxide (N₂O) vibrational overtone transition

Gang Zhao ^{1,*} D. Michelle Bailey ¹ Adam J. Fleisher ^{1,†} Joseph T. Hodges ¹ and Kevin K. Lehmann ²

¹National Institute of Standards and Technology, 100 Bureau Drive, Gaithersburg, Maryland 20899, USA

²Departments of Chemistry and Physics, University of Virginia, Charlottesville, Virginia 22904, USA



(Received 27 March 2020; accepted 14 May 2020; published 4 June 2020)

We report Doppler-free two-photon absorption of N₂O at $\lambda = 4.53 \mu\text{m}$, measured by cavity ring-down spectroscopy. High power was achieved by optical self-locking of a quantum cascade laser to a linear resonator of finesse $\mathcal{F} = 22730$, and accurate laser detuning over a 400-MHz range was measured relative to an optical frequency comb. At a sample pressure of $p = 0.13 \text{ kPa}$, we report a large two-photon cross section per molecule of $\sigma_{13}^{(2)} = 8.0 \times 10^{-41} \text{ cm}^4 \text{ s}$ for the $Q(18)$ rovibrational transition at a resonant frequency of $\nu_0 = 66179400.8 \text{ MHz}$.

DOI: [10.1103/PhysRevA.101.062509](https://doi.org/10.1103/PhysRevA.101.062509)

I. INTRODUCTION

Two-photon spectroscopy of the $1S$ - $2S$ transition of hydrogen (H) has inspired 45 years of precision laser measurements [1–3]. The fractional uncertainty in this transition frequency is currently 4.2×10^{-15} [4], a record enabled by remarkable advances in tools for frequency metrology and control like the optical frequency comb [2,5]. In general, two-photon absorption [6,7] by counterpropagating beams of identical frequency eliminates the first-order Doppler effect [8,9], resulting in ultranarrow lines with homogeneous broadening ultimately limited by the natural lifetime of the upper state—ideal for precision spectroscopy. Consequently, two-photon spectroscopy remains at the forefront of several challenges in modern physics [10], including tests of charge-parity-time symmetry using antihydrogen [11] and attempts to solve the proton-size puzzle [12].

With additional degrees of freedom, molecules also possess two-photon absorption lines throughout the electromagnetic spectrum. However, only molecules with fortuitous transition frequencies near the emission lines of high-powered gas lasers have been observed [13–15]. Specifically, infrared absorption cross sections are generally smaller than those associated with electronic transitions, so new infrared techniques with substantially greater sensitivity are required. Nevertheless, several intriguing tests of fundamental physics enabled by molecules await, like the search for parity violations in chiral species [16] and tests of fundamental constants by hydrogen molecular ions [17]. The theories associated with these tests have motivated recent advances in tunable infrared lasers with state-of-the-art frequency accuracy [18–20].

Here we report Doppler-free two-photon absorption of the $Q(18)$ rovibrational transition within the ν_3 overtone band of N₂O, measured by cavity ring-down spectroscopy (CRDS) at a wavelength of $\lambda = 4.53 \mu\text{m}$. As proposed by Lehmann in Ref. [21], we demonstrate two-photon CRDS to be a sensitive probe for selected light-matter interactions within an optical cavity. Resonance enhanced two-photon CRDS has a distinct sensitivity advantage over saturated absorption techniques [22–25], where the former Doppler-free process benefits from a near degeneracy of energy levels and the fact that all velocity classes contribute to the two-photon cross section. Here we directly measured the resonance enhanced two-photon absorption rate for a chosen N₂O transition, as well as its transition frequency, pressure shift, and collisional air-broadening coefficient. Furthermore, we project an N₂O detection limit which is 125-fold better than current laser gas analyzers using cavity-enhanced linear absorption techniques.

These measurements required the creation of a cavity-locked quantum cascade laser (QCL) spectrometer with tunable frequency axis referenced to a stabilized optical frequency comb. The spectrometer, with ultranarrow relative linewidth and high circulating power, comprised a semiconductor laser controlled by an optical-electronic phase-locking scheme.

II. RESULTS

The experimental setup shown in Fig. 1(a) was developed and implemented at the National Institute of Standards and Technology (NIST) in Gaithersburg, Maryland. The continuous-wave distributed feedback QCL (HHL-14-75, AdTech Optics) with antireflection coated output facet emitted at $\lambda = 4.53 \mu\text{m}$ with a collimated output power of $\sim 100 \text{ mW}$. The QCL drive current was modulated by a sinusoidal signal at 1.8 MHz to create sidebands for electronic stabilization of the round-trip feedback phase. A pair of lenses, i.e., lens₁ and lens₂, were used to perform spatial mode-matching to a Fabry-Pérot type linear optical resonator (or cavity). The cavity comprised two planoconcave mirrors with 1-m radius

*Permanent address: Institute of Laser Spectroscopy, State Key Laboratory of Quantum Optics and Quantum Devices, Shanxi University, Taiyuan City 030006, Shanxi Province, People's Republic of China

†adam.fleisher@nist.gov

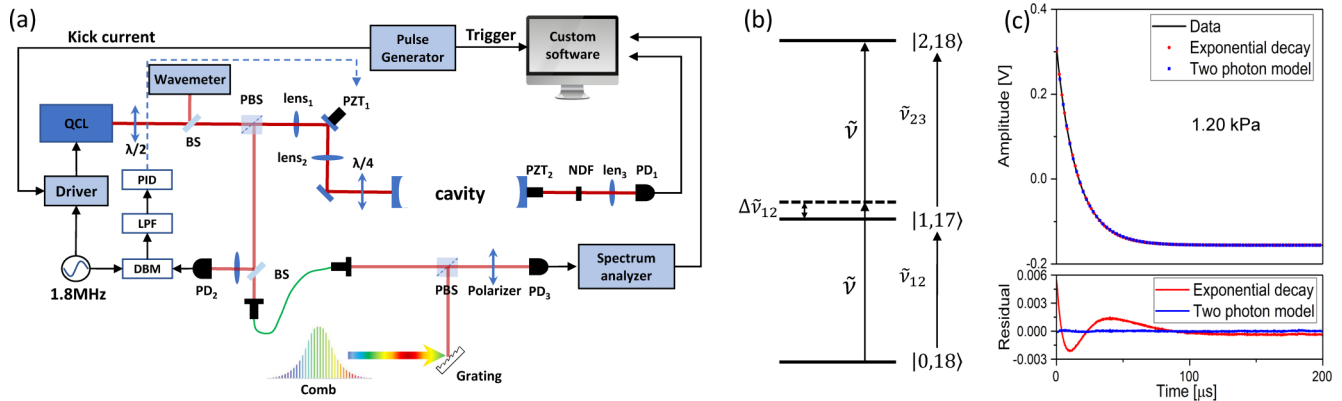


FIG. 1. (a) Experimental setup. QCL, quantum cascade laser; $\lambda/2$, half-wave plate; $\lambda/4$, quarter-wave plate; BS, beam splitter; PZT, piezoelectric transducer; NDF, neutral density filter; PD, photodetector; DBM, double-balanced mixer; LPF, low-pass filter; PID, proportional-integral-derivative. (b) Resonance enhanced $Q(18)$ two-photon transition, ν_3 vibrational ladder of N_2O . Quantum states, $|\nu_3, J\rangle$. (c) Upper panel. Cavity ring-down signal, $24.8 \mu\text{mol mol}^{-1}$ N_2O -in-air, pressure $p = 1.20$ kPa (black line). Exponential (red dots) and two-photon (blue dots) fitted models. Lower panel. Fitted residuals.

of curvature separated by a stainless-steel vacuum enclosure with invar support rods, resulting in an optical single-pass cavity length of nominally $L = 75$ cm, free spectral range of 200 MHz, and beam waist radius at the focus of 0.835 mm.

QCL locking to the cavity was realized by optical feedback from the cavity leak-out field in a configuration similar to Ref. [26] and without any need for intentional mode mismatching [27–29]. The feedback ratio could be adjusted without loss of incident power to the cavity by rotating a quarter-wave plate ($\lambda/4$) to change the deflection ratio of the reflected light at the polarizing beam splitter (PBS). Stable feedback was established when the fast axis of $\lambda/4$ was rotated $\sim 45^\circ$ relative to the transmission axis of the PBS, resulting in circularly polarized light entering the cavity and an estimated feedback fractional intensity of $\sim 10^{-4}$. The feedback phase condition was initially satisfied by adjusting the length between the laser and the cavity to approximately equal the cavity length L . Then, electronic phase stabilization was added by controlling the laser-cavity path length using a piezomounted mirror (PZT₁) in the light propagation path driven by a proportional-integral-derivative servo with a cascaded double-integral circuit (D2-125, Vescent Photonics). The error signal was generated in a manner similar to Ref. [30], i.e., by demodulating the reflected light deflected by PBS and received by photodetector PD₂.

The mirror power reflectivity (\mathcal{R}), transmittivity (\mathcal{T}), and combined loss coefficients (\mathcal{L} , absorption and scattering), as well as the fraction of the incident power coupled into the lowest order transverse cavity mode (ε) were estimated by measuring the empty-cavity ring-down time, the optical power reflected from the cavity both on- and off-resonance, the incident power, and the transmitted on-resonance power. From those measurements, we inferred [31,32]: $\mathcal{R} = 0.9998618$, $\mathcal{T} = 6.99 \times 10^{-5}$, $\mathcal{L} = 6.83 \times 10^{-5}$, and $\varepsilon = 0.54$. The calculated cavity finesse was 22730 with a standard uncertainty of 160. On resonance and at an incident power of 26 mW, the empty-cavity transmitted power was measured to be 4.1 mW, which implies a one-way intracavity power of 60 W.

Cavity decay signals were measured in transmission by a liquid-nitrogen-cooled InSb photoconductive detector (PD₁,

responsivity of 3.5 A/W) following a neutral density filter (NDF) with optical density $OD = 1.2$. Detector response was converted to voltage by a transimpedance amplifier and then digitized by an oscilloscope card (PCI5922, National Instruments) with 18-bit resolution at a sampling rate of 10^7 s^{-1} . The cavity-locked laser frequency could be continuously tuned over a range of 400 MHz by changing the voltage to a piezo-electric transducer (PZT₂) attached to one of the cavity mirrors. Low and high precision values for the laser wavelength were determined, respectively, by a wavelength meter (721, Bristol) and by beating with a stabilized frequency comb (Menlo Systems). The frequency comb was an offset-free difference frequency generation system ($f_0 = 0$) with repetition rate $f_{\text{rep}} = 250$ MHz when locked to a Rb clock signal (SIM940, Stanford Research Systems, short-term stability of $< 2 \times 10^{-11}$ at 1 s). The beat note frequency was recorded by a spectrum analyzer and processed by a custom software program to calculate the laser frequency at each point of the two-photon spectra relative to the comb.

Decay events were triggered by rapidly changing the QCL drive current, thus breaking the optical-electronic phase-locked loop. The two-photon transition of $^{14}N_2^{16}O$ at a calculated wave number of $\tilde{\nu}_0 = 2207.507 \text{ cm}^{-1}$ was chosen because of strong resonance enhancement between the $P(18)$ transition of the ν_3 fundamental and the $R(17)$ transition of the first ν_3 vibrational hot band [Fig. 1(b)]. The intermediate state is detuned by only 0.113 cm^{-1} from the predicted resonant frequency of the two-photon transition, resulting in a calculated two-photon cross section at 296 K and 0.13 kPa of $\sigma_{13}^{(2)} = 5.9 \times 10^{-41} \text{ cm}^4 \text{ s molecule}^{-1}$.

The gas sample comprised $24.8069 \mu\text{mol/mol} \pm 0.0076 \mu\text{mol/mol}$ N_2O in air (expanded uncertainty, or coverage factor $k = 2$, cylinder # FB03344), and was gravimetrically prepared at NIST using synthetic air of largely O_2 and N_2 [33]. Sample temperature (T_g) and pressure (p) were measured by two platinum resistance thermometers in good thermal contact with the outside of the sample cell and a 1.3 kPa full-scale pressure gauge, respectively, each of which was calibrated against secondary NIST standards.

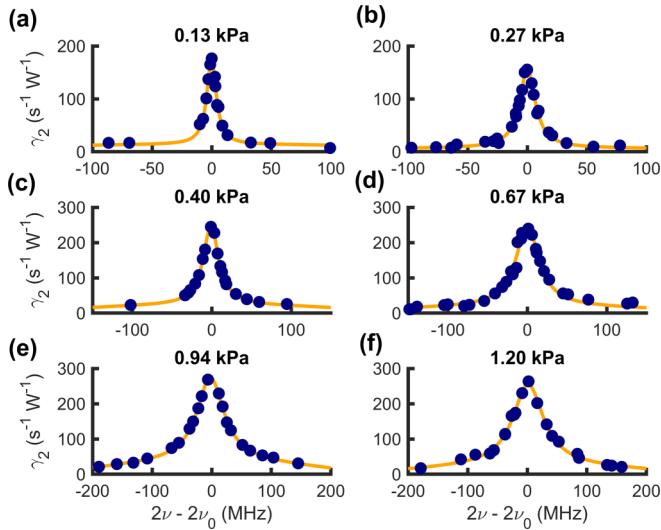


FIG. 2. Measured γ_2 as a function of two-photon detuning $2\nu - 2\nu_0$ for the N_2O $Q(18)$ ν_3 overtone transition. (a)–(f) Panels labeled by p . Resonant two-photon transition frequency, $\nu_0 = 66179400.8 \text{ MHz} \pm 0.3 \text{ MHz}$.

The black line in Fig. 1(c) shows the measured two-photon ring-down signal at 1.20 kPa of N_2O -in-air, triggered near the center of the $Q(18)$ ν_3 transition. Red and blue dots show the fitted exponential decay and two-photon cavity ring-down models, respectively. The two-photon ring-down model [21,23] is reproduced below in Eq. (1), and the fit in Fig. 1(c) involved floating the following parameters: γ_1 , γ_2 , the voltage at the detector at zero time $V_{\text{det}}(0)$, and a detector offset V_0

$$V_{\text{det}}(t) = \frac{\gamma_1 V_{\text{det}}(0) \exp(-\gamma_1 t)}{\gamma_1 + \gamma_2 \left(\frac{V_{\text{det}}(0)}{G_d \mathcal{J}} \right) (1 - \exp(-\gamma_1 t))} + V_0. \quad (1)$$

The quantity $V_{\text{det}}(0)/(G_d \mathcal{J})$ is equal to the intracavity power at zero time $P_{\text{ic}}(0)$ in units of W, where $G_d = 215 \text{ V W}^{-1}$ is the measured gain of the detection system including the transmittance associated with the neutral density filter (NDF) shown in Fig. 1(a). Also in Eq. (1), $V_{\text{det}}(t)$ is the voltage measured by the detection system as function of time (t) in units of V, γ_1 is the one-photon absorption rate (which includes both mirror losses and linear molecular losses) in units of s^{-1} , and γ_2 is the two-photon absorption rate in units of $\text{s}^{-1} \text{ W}^{-1}$. Shown in the lower panel of Fig. 1(c) are the fitted residuals corresponding to each model. Systematic structure in the residuals of the exponential decay model, with maximum deviation of up to 2% of $V_{\text{det}}(0)$, illustrates the presence of strong nonlinear absorption. In contrast, fitting with two-photon ring-down model yielded low root-mean-square (RMS) noise. Defining the ring-down signal-to-noise ratio (SNR) as the signal at zero time divided by the RMS noise, we observed $\text{SNR} = 6.5 \times 10^3$ for one decay event.

The two-photon spectrum of N_2O over the frequency interval of $\pm 200 \text{ MHz}$ about the center of the transition was acquired by adjusting the cavity PZT_2 voltage to tune the laser frequency. To eliminate correlation between γ_1 and γ_2 observed while fitting individual two-photon decay signals (correlation coefficient, $\rho_{12} \approx -0.95$), we constrained

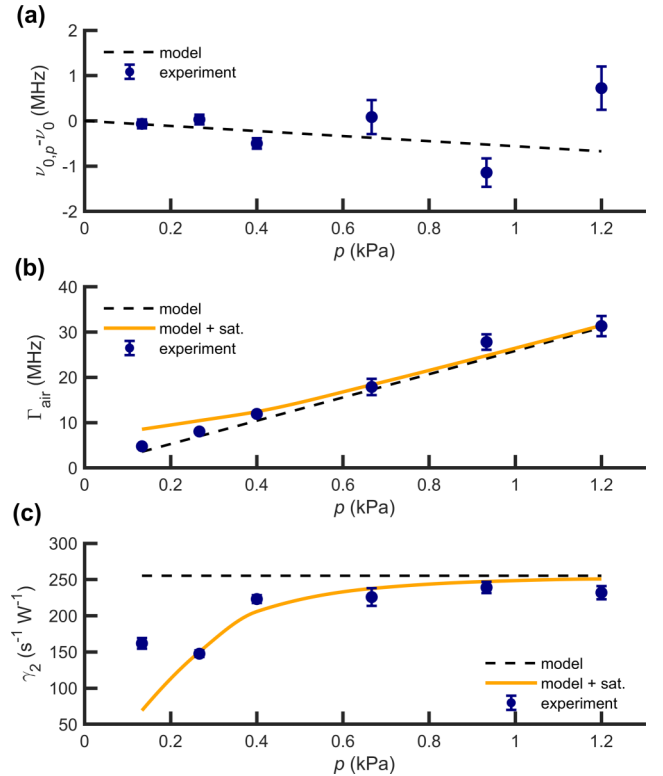


FIG. 3. (a) Fitted resonant frequencies $\nu_{0,p}$ for the two-photon transition vs p . Black dashed line, weighted linear fit. (b). Two-photon half width at half maximum (Γ_{air}) vs p . Orange line, fitted air-broadening coefficient including power broadening. Black dashed line, model without power broadening (c). Two-photon absorption rate (γ_2) vs p . Orange line, fitted γ_2 including saturation. Black dashed line, fitted value of γ_2 without saturation.

γ_1 to be a linear function of frequency detuning. The linear constraint captured frequency-dependent losses from the far wing of the $P(18)$ fundamental transition as well as spatially dependent changes in mirror losses. We also fixed the initial voltage $V_{\text{det}}(0)$ to equal the first data point in each decay and fixed the offset term V_0 to equal the average of the final ten data points in the decay. Therefore, γ_2 was the only model parameter floated in Eq. (1) during spectral analysis.

Two-photon spectra, recorded at six different gas sample pressures from 0.13 to 1.20 kPa, are shown in Fig. 2 (dark blue dots), along with their corresponding fitted models (orange lines, Lorentzian line shape function, Doppler-broadened pedestal [3]). The resonant two-photon transition frequency was calculated at zero pressure from a linear fit of the data in Fig. 2: $\nu_0 = 66179400.8 \text{ MHz} \pm 0.3 \text{ MHz}$ (tenfold lower statistical uncertainty than HITRAN 2016 [34]).

Pressure-dependent values for the resonant two-photon transition frequency ($\nu_{0,p}$) are plotted versus p in Fig. 3(a). Throughout Fig. 3, expanded ($k = 2$) statistical uncertainties from the fitting process are shown. The transition frequencies are reported relative to the value at zero pressure, i.e., $\nu_{0,p} - \nu_0$, where ν_0 and the pressure shift coefficient δ_{air} resulted from a weighted linear fit, i.e., the black dashed line. The measured pressure shift for the resonant frequency of the two-photon transition is $\delta_{\text{air}} = -0.6 \text{ MHz kPa}^{-1} \pm$

TABLE I. Summary of fitted two-photon absorption parameters along with database calculations using HITRAN2016 data [34] and equations in Ref. [21]. Two-photon absorption cross sections ($\sigma_{13}^{(2)}$) were calculated per molecule of N_2O and correspond to $p = 0.13$ kPa.

Parameter	Units	Measured value	Statistical uncertainty ($k = 1$)	Database calculation
ν_0	MHz	66179400.8	0.3	66179401
δ_{air}	MHz kPa $^{-1}$	-0.6	0.8	-0.63
b_p	MHz kPa $^{-1}$	25.7	1.2	22.5
$\sigma_{13}^{(2)}$	cm 4 s molecule $^{-1}$	8.0×10^{-41}	0.2×10^{-41}	5.9×10^{-41}

0.8 MHz kPa $^{-1}$, comparable to the average pressure shift reported in HITRAN2016 [34] for the two near-degenerate one-photon transitions, $\delta_{\text{air}} = -0.63$ MHz kPa $^{-1}$.

The fitted two-photon homogeneous broadening (Γ_{air}) as a function of p is plotted in Fig. 3(b). The orange line, with fitted air-broadening coefficient $b_p = 25.7$ MHz kPa $^{-1} \pm 1.2$ MHz kPa $^{-1}$, includes an estimate for two-photon saturation [21]. For comparison, the air-broadening coefficients (half width at half maximum) for both the near-resonant one-photon transitions are $b_p^{(1)} = 22.5$ MHz kPa $^{-1}$ [34]. While fitting the orange line, Γ_{air} at zero pressure was fixed to be twice the sum of our absolute laser linewidth (~ 270 kHz at 1 s) and the calculated transit-time broadening (30 kHz). Collisional air-broadening without saturation is predicted by the black dashed line.

Our transition frequency and collisional air-broadening analyses ignored unresolved nuclear quadrupole hyperfine structure attributable to each nitrogen atom, as well as any AC Stark shift. Further, we also ignored potential quantum-interference effects and one-photon saturation, including from the far-wing of the one-photon $P(18)$ ν_3 fundamental transition that participates in the two-photon resonance enhancement.

Values of γ_2 fitted at ν_0 (dark blue dots) are plotted in Fig. 3(c) along with the theoretical values calculated from Eq. (2) (black dashed line):

$$\gamma_2 = \frac{A_{12}A_{23}a_p(J_1, J_2, J_3)\chi_a f_1}{256\pi^4 hc^3 L k_B T_g \Delta \tilde{\nu}_{12}^2 \tilde{\nu}^4 b_p}. \quad (2)$$

Details regarding Eq. (2), derived in the limit of a confocal cavity and valid only when the near degeneracy ($\Delta \tilde{\nu}_{12} = \tilde{\nu}_{12} - \tilde{\nu}$) is much greater than both the one-photon Doppler and collisional broadening, are available in Ref. [21]. Briefly, A_{12} and A_{23} are the Einstein coefficients for spontaneous emission, a_p is a polarization-dependent factor calculated from Table II of Ref. [21], χ_a is the known mole fraction of absorbers, f_1 is the Boltzmann factor for selected isotopologue or isotopomer in its lower state, h is the Planck constant, c is the speed of light, L is the known cavity length, k_B is the Boltzmann constant, T_g is the measured gas temperature, $\tilde{\nu}$ is the resonant wave number of the two-photon transition, and b_p is the measured two-photon collisional air-broadening coefficient.

At high pressures in Fig. 3(c), the experimental values of γ_2 approach a constant value of $255 \text{ s}^{-1} \text{ W}^{-1} \pm 7 \text{ s}^{-1} \text{ W}^{-1}$. The orange line shows the fitted γ_2 including saturation of the two-photon transition, i.e., multiplying Eq. (2) by a factor of $1/(1 + G_{\text{TP}}^2)$, where G_{TP} is the degree of two-photon saturation $G_{\text{TP}} = P_{\text{ic}}/P_{\text{sat}}$. In Ref. [21], P_{sat} for the two-photon

transition is predicted to be proportional to p in the collisional broadening regime. However, that prediction may overestimate the saturation power due to its neglect of expected very slow vibrational-to-translational and vibrational-to-rotational relaxation (e.g., Ref. [35]). Fitted two-photon absorption parameters are summarized in Table I.

At $p = 1.20$ kPa, where γ_2 approaches the asymptotic value shown in Fig. 3(c), we observed a cavity transmitted power of 1.8 mW corresponding to an intracavity power of $P_{\text{ic}}(0) = 26$ W and a power at PD $_1$ of $P_{\text{det}}(0) = 110 \mu\text{W}$ —recalling that $\text{OD} = 1.2$ for the NDF shown in Fig. 1(a). From the predicted standard error of two-photon absorption coefficient α_2 [21,23], we calculate for our observations—single ring-down events with noise-equivalent power $P_N \leq 120$ nW dominated by systematic sources—a minimum α_2 of $1.6 \times 10^{-12} \text{ cm}^{-1} \text{ W}^{-1}$. This value is fourfold larger than the shot-noise limited sensitivity and tenfold larger than the technical-noise limited sensitivity (both calculated from Eq. (12) of Ref. [23], with our technical noise dominated by the transimpedance amplifier and oscilloscope card). Assuming an acquisition rate of $f_{\text{acq}} = \gamma_1/10 \approx 5.5$ kHz and eliminating the NDF, i.e., $P_{\text{det}}(0) = 1.8$ mW, we project [21] a shot-noise-equivalent α_2 for our spectrometer of $\sigma(\gamma_2)/(c\sqrt{f_{\text{acq}}}) = 2.7 \times 10^{-15} \text{ cm}^{-1} \text{ W}^{-1} \text{ Hz}^{-1/2}$, where $\sigma(\gamma_2)$ is the standard error in γ_2 . This result is equivalent to a 1 s N_2O detection limit of $\sigma_{\text{N}_2\text{O}}(1 \text{ s}) = 7.9 \text{ pmol mol}^{-1} \text{ Hz}^{-1/2}$.

A recent intercomparison of analytical instruments reported sensitivity limits for N_2O mole fraction [36]. The study included laser gas analyzers operating near $\lambda = 4.53 \mu\text{m}$, which utilized linear absorption techniques like CRDS, off-axis integrated cavity output spectroscopy, and long path-length quantum cascade laser absorption spectroscopy. For a gas sample with N_2O mole fraction of $10 \mu\text{mol mol}^{-1}$, comparable to our sample of $24.8 \mu\text{mol mol}^{-1}$, they observed 1-s precision values as low as $\sigma_{\text{N}_2\text{O}}(1 \text{ s}) = 1 \text{ nmol mol}^{-1} \text{ Hz}^{-1/2}$. If achieved, our shot-noise limited projection would outperform the best linear absorption analyzer in that study by 125-fold, thus illustrating the extreme sensitivity limits of two-photon CRDS enabled by optical-electronic QCL stabilization. Further, two-photon CRDS promises intrinsic long-term stability by simultaneously measuring linear absorption and two-photon rates.

III. CONCLUSIONS

Cavity ring-down spectroscopy possesses several well-known advantages over conventional detection approaches. Specifically, it measures the photon decay rate that is easily related to the loss per unit length. Also, the passive decay signals are immune to laser intensity noise, and decay rates

can be retrieved with shot-noise limited sensitivity [37] and metrology-grade accuracy [38]. Here we have demonstrated that the high circulating power and counterpropagating laser fields characteristic of cavity ring-down spectroscopy can yield intense, velocity-class-indiscriminate, Doppler-free two-photon absorption spectra.

Improving upon our first measurements is relatively straightforward. Laser stabilization to an independent reference cavity will eliminate complications associated with disrupting our phase-locked loop to initiate decays. This will enable acquisition rates limited by the one-photon decay rate, and the inclusion of a high extinction ratio optical switch, e.g., an acousto-optic modulator, will reduce uncertainty in fitted two-photon decay rates. We also anticipate improved tunability over a larger dynamic range of intracavity powers. Further phase stabilization of the laser to an absolute frequency reference would improve spectrometer fidelity and enable longer integration times and an assessment of overall

accuracy. Consequently, and combined with broadly tunable stabilized lasers throughout the midinfrared achieved by either the phase-locking approach demonstrated here or another more elaborate scheme (e.g., Refs. [18–20]), two-photon cavity ring-down spectroscopy as a tool at the vanguard of modern molecular physics is on the horizon.

ACKNOWLEDGMENTS

We acknowledge technical assistance from Q. Liu (NIST) during optical resonator design, fabrication, and assembly, and C. E. Cecelski (NIST) and J. Carney (NIST) for the loan of a certified gas sample of N₂O-in-air. H. M. Fleurbaey (NIST) commented on the manuscript. The work was funded by the National Institute of Standards and Technology (NIST), the National Research Council (NRC) Postdoctoral Research Associateships Program, and the University of Virginia.

-
- [1] T. W. Hänsch, S. A. Lee, R. Wallenstein, and C. Wieman, Doppler-Free Two-Photon Spectroscopy of Hydrogen 1S-2S, *Phys. Rev. Lett.* **34**, 307 (1975).
 - [2] T. W. Hänsch, Nobel lecture: Passion for precision, *Rev. Mod. Phys.* **78**, 1297 (2006).
 - [3] F. Biraben, The first decades of Doppler-free two-photon spectroscopy, *C. R. Phys.* **20**, 671 (2019).
 - [4] C. G. Parthey, A. Matveev, J. Alnis, B. Bernhardt, A. Beyer, R. Holzwarth, A. Maistrou, R. Pohl, K. Predehl, T. Udem *et al.*, Improved Measurement of the Hydrogen 1S-2S Transition Frequency, *Phys. Rev. Lett.* **107**, 203001 (2011).
 - [5] J. L. Hall, Nobel lecture: Defining and measuring optical frequencies, *Rev. Mod. Phys.* **78**, 1279 (2006).
 - [6] M. Göppert-Mayer, Über elementarakte mit zwei quantensprüngen, *Ann. Phys.* **401**, 273 (1931).
 - [7] W. Kaiser and C. G. B. Garrett, Two-Photon Excitation in CaF₂:Eu²⁺, *Phys. Rev. Lett.* **7**, 229 (1961).
 - [8] L. S. Vasilenko, V. P. Chebotayev, and A. V. Shishaev, Line shape of two-photon absorption in a standing-wave field in a gas, *JETP Lett.* **12**, 113 (1970).
 - [9] B. Cagnac, G. Grynberg, and F. Biraben, Spectroscopie d'absorption multiphotonique sans effet Doppler, *J. Phys. France* **34**, 845 (1973).
 - [10] M. S. Safronova, D. Budker, D. DeMille, D. F. Jackson Kimball, A. Derevianko, and C. W. Clark, Search for new physics with atoms and molecules, *Rev. Mod. Phys.* **90**, 025008 (2018).
 - [11] The ALPHA Collaboration, Characterization of the 1S-2S transition in antihydrogen, *Nature (London)* **557**, 71 (2018).
 - [12] H. Fleurbaey, S. Galtier, S. Thomas, M. Bonnaud, L. Julien, F. Biraben, F. Nez, M. Abgrall, and J. Guéna, New Measurement of the 1S-3S Transition Frequency of Hydrogen: Contribution to the Proton Charge Radius Puzzle, *Phys. Rev. Lett.* **120**, 183001 (2018).
 - [13] W. K. Bischel, P. J. Kelly, and C. K. Rhodes, High resolution Doppler-free two-photon spectroscopic studies of molecules. I. The ν_3 bands of ¹²CH₃F, *Phys. Rev. A* **13**, 1817 (1976).
 - [14] W. K. Bischel, P. J. Kelly, and C. K. Rhodes, High resolution Doppler-free two-photon spectroscopic studies of molecules. II. The ν_2 bands of ¹⁴NH₃, *Phys. Rev. A* **13**, 1829 (1976).
 - [15] F. Herlemont, M. Lyszyk, and J. Lemaire, Doppler-free two-photon spectroscopy of the $2\nu_3$ band of SF₆, *Appl. Phys.* **24**, 369 (1981).
 - [16] S. K. Tokunaga, C. Stoeffler, F. Auguste, A. Shelkownikov, C. Daussy, A. Amy-Klein, C. Chardonnet, and B. Darquié, Probing weak force-induced parity violation by high-resolution mid-infrared molecular spectroscopy, *Mol. Phys.* **111**, 2363 (2013).
 - [17] J.-Ph. Karr, L. Hilico, J. C. J. Koelemeij, and V. I. Korobov, Hydrogen molecular ions for improved determination of fundamental constants, *Phys. Rev. A* **94**, 050501(R) (2016).
 - [18] B. Argence, B. Chanteau, O. Lopez, D. Nicolodi, M. Abgrall, C. Chardonnet, C. Daussy, B. Darquié, Y. Le Coq, and A. Amy-Klein, Quantum cascade laser frequency stabilization at the sub-Hz level, *Nat. Photon.* **9**, 456 (2015).
 - [19] R. Santagata, D. B. A. Tran, B. Argence, O. Lopez, S. K. Tokunga, F. Wiotte, H. Mouhamad, A. Goncharov, M. Abgrall, Y. Le Coq *et al.*, High-precision methanol spectroscopy with a widely tunable SI-traceable frequency-comb-based mid-infrared QCL, *Optica* **6**, 411 (2019).
 - [20] S. Borri, G. Insero, G. Santambrogio, D. Mazzotti, F. Cappelli, I. Galli, G. Galzerano, M. Marangoni, P. Laporta, V. Di Sarno *et al.*, High-precision molecular spectroscopy in the mid-infrared using quantum cascade lasers, *Appl. Phys. B* **125**, 18 (2019).
 - [21] K. K. Lehmann, Resonance enhanced two-photon cavity ring-down spectroscopy of vibrational overtone bands: A proposal, *J. Chem. Phys.* **151**, 144201 (2019).
 - [22] G. Giusfredi, S. Bartalini, S. Borri, P. Cancio, I. Galli, D. Mazzotti, and P. De Natale, Saturated-Absorption Cavity Ring-Down Spectroscopy, *Phys. Rev. Lett.* **104**, 110801 (2010).
 - [23] K. K. Lehmann, Theoretical detection limits of saturated absorption cavity ring-down spectroscopy (SCAR) and two-photon absorption cavity ring-down spectroscopy, *Appl. Phys. B* **116**, 147 (2014).
 - [24] G. Giusfredi, I. Galli, D. Mazzotti, P. Cancio, and P. De Natale, Theory of saturated-absorption cavity ring-down: Radiocarbon dioxide detection, a case study, *J. Opt. Soc. Am. B* **32**, 2223 (2015).

- [25] I. Sadiq and G. Friedrichs, Saturation dynamics and working limits of saturated absorption cavity ringdown spectroscopy, *Phys. Chem. Chem. Phys.* **18**, 22978 (2016).
- [26] M. Durand, J. Morville, and D. Romanini, Shot-noise-limited measurement of sub-parts-per-trillion birefringence phase shift in a high-finesse cavity, *Phys. Rev. A* **82**, 031803(R) (2010).
- [27] D. A. King and R. J. Pittaro, Simple diode pumping of a power-buildup cavity, *Opt. Lett.* **23**, 774 (1998).
- [28] A. G. V. Bergin, G. Hancock, G. A. D. Ritchie, and D. Weidmann, Linear cavity optical-feedback cavity-enhanced absorption spectroscopy with a quantum cascade laser, *Opt. Lett.* **38**, 2475 (2013).
- [29] K. M. Manfred, L. Ciaffoni, and G. A. D. Ritchie, Optical-feedback cavity-enhanced absorption spectroscopy in a linear cavity: model and experiments, *Appl. Phys. B* **120**, 329 (2015).
- [30] A. Hemmerich, D. H. McIntyre, D. Schropp, D. Meschede, and T. W. Hänsch, Optically stabilized narrow linewidth semiconductor laser for high resolution spectroscopy, *Opt. Commun.* **75**, 118 (1989).
- [31] C. J. Hood, H. J. Kimble, and J. Ye, Characterization of high-finesse mirrors: Loss, phase shifts, and mode structure in an optical cavity, *Phys. Rev. A* **64**, 033804 (2001).
- [32] G. Zhao, T. Hausmaninger, W. Ma, and O. Axner, Differential noise-immune cavity ring-down optical heterodyne molecular spectroscopy for improvement of the detection sensitivity by reduction of drifts from background signals, *Opt. Express* **25**, 29454 (2017).
- [33] M. E. Kelly, G. C. Rhoderick, and F. R. Guenther, Development and verification of air balance gas primary standards for measurement of nitrous oxide at atmospheric levels, *Anal. Chem.* **86**, 4544 (2014).
- [34] I. E. Gordon, L. S. Rothman, C. Hill, R. V. Kochanov, Y. Tan, P. F. Bernath, M. Birk, V. Boudon, A. Campargue, K. V. Chance *et al.*, The HITRAN2016 molecular spectroscopic database, *J. Quant. Spectrosc. Radiat. Transfer* **203**, 3 (2017).
- [35] T. Hausmaninger, G. Zhao, W. Ma, and O. Axner, Depletion of the vibrational ground state of CH₄ in absorption spectroscopy at 3.4 μm in N₂ and air in the 1 Torr range, *J. Quant. Spectrosc. Radiat. Transfer* **205**, 59 (2018).
- [36] S. J. Harris, J. Liisberg, L. Xia, J. Wei, K. Zeyer, L. Yu, M. Barthel, B. Wolf, B. F. J. Kelly, D. I. Cendón *et al.*, N₂O isotopologue measurements using laser spectroscopy: Analyzer characterization and intercomparison, *Atmos. Meas. Tech.* **13**, 2797 (2020).
- [37] D. A. Long, A. J. Fleisher, Q. Liu, and J. T. Hodges, Ultra-sensitive cavity ring-down spectroscopy in the mid-infrared spectral region, *Opt. Lett.* **41**, 1612 (2016).
- [38] A. J. Fleisher, E. M. Adkins, Z. D. Reed, H. Yi, D. A. Long, H. M. Fleurbaey, and J. T. Hodges, Twenty-Five-Fold Reduction in Measurement Uncertainty for a Molecular Line Intensity, *Phys. Rev. Lett.* **123**, 043001 (2019).